ACS OMEGA

Article

Cite This: ACS Omega 2020, 5, 626−633

http://pubs.acs.org/journal/acsodf

Implications of Testing a Zinc−Oxygen Battery with Zinc Foil Anode Revealed by Operando Gas Analysis

Saustin Dongmo,[†,‡] Daniel Stock,[†,‡] Julian Jakob Alexander Kreissl,[†] Martin Groß,[§] Sophie Weixler,[§] Markus Hagen,[§] Kohei Miyazaki,[∥] Takeshi Abe,[∥] and Daniel Schröder*[,†,‡]

[†]Institute of Physical Chemistry, Justus Liebig University Giessen, Heinrich-Buff-Ring 17, D-35392 Giessen, Germany

[‡]Center for Materials Research (LaMa), Justus Liebig University Giessen, Heinrich-Buff-Ring 16, D-35392 Giessen, Germany

[§]Fraunhofer Institute for Chemical Technology ICT, Joseph-von-Fraunhofer-Straße 7, D-76327 Pfinztal, Germany

[∥]Department of Energy & Hydrocarbon Chemistry, Kyoto University, Nishikyo-ku, 615-8510 Kyoto, Japan

Supporting Information

ABSTRACT: Zinc−oxygen batteries are seen as promising energy storage devices for future mobile and stationary applications. Introducing them as secondary battery is hindered by issues at both the anode and cathode. Research efforts were intensified during the past two decades, mainly focusing on catalyst materials for the cathode. Thereby, zinc foil was almost exclusively used as the anode in electrochemical testing in the lab-scale as it is easy to apply and shall yield reproducible results. However, it is well known that zinc metal reacts with water within the electrolyte to form hydrogen. It is not yet clear how the evolution of hydrogen is affecting the performance results obtained thereof. Herein, we extend the studies and the understanding about the evolution of hydrogen at zinc by analyzing the zinc−oxygen battery during operation. By means of electrochemical measurements, operando gas analysis, and anode surface analysis, we elucidate that the rate of the evolution of hydrogen scales with the current density applied, and that the roughness of the anode surface, that is, the pristine state of the zinc foil surface, affects the rate as well. In the end, we propose a link between the evolution of hydrogen and the unwanted impact on the actual electrochemical performance that might go unnoticed during testing. Thereof, we elucidate the consequences that arise for the working principle and the testing of materials for this battery type.

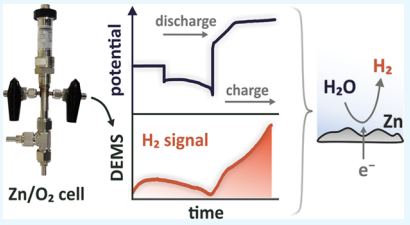

INTRODUCTION

Metal−oxygen batteries are seen as promising energy storage devices and possess theoretical energy densities that can be higher than that of lithium-ion batteries.[1,2] However, their application as electrically rechargeable battery technology—both for aqueous metal−oxygen batteries and nonaqueous metal−oxygen batteries—is hindered so far because fundamental and technical challenges remain.[3−6] Major drawbacks are energy efficiency, the need for purified oxygen, as well as the poor cycle life due to electrolyte decomposition.[7,8] Especially, in the case of organic Li−O_2 batteries, it is well known that high overpotentials during charge decompose the organic electrolyte.[9−11] Thereby, using operando techniques allows better understanding the processes involved.[12−17]

Among the aqueous metal−oxygen batteries, the alkaline zinc−oxygen (Zn−O_2) battery has been seen as highly promising[8,18−20] but exhibits a similar, equally grave side reaction: the evolution of hydrogen (HER) on the active material Zn occurs because Zn is reacting with water from the alkaline aqueous electrolyte to form hydrogen (H_2) and zinc hydroxide species ($Zn(OH)_2$)[21−23] as follows

$$Zn + 2H_2O \rightarrow Zn(OH)_2 + H_2\uparrow \quad (1)$$

Thereby, not only the solvent in the electrolyte is consumed and gas bubbles are formed but the precious active material Zn at the anode is converted to an inactive, insulating material in the process. This loss of active material ultimately leads to a severe decrease in usable capacity. A detailed description of the working principle of the Zn−O_2 battery is provided in the Supporting Information (see reactions S1−S3).

The HER is considered since decades to be responsible for the self-discharge of the Zn−O_2 battery.[24−27] Efficient strategies were developed to suppress the HER and thus to diminish the degradation of the anode.[28] The strategies aim to reduce the activity of H_2O and hence the rate of the HER, for example, by adding inorganic and organic inhibitors to the Zn metal powder or paste or by using metal alloys as the Zn anode.[24,25,29−32] It is well known that the "HER also consumes electrons during the charging process" (Chen et al.[33]) and that the electrons could rather be invested into the HER if all ZnO is converted back to Zn.

Interestingly, the major research focus for Zn−O_2 batteries is on cathode materials and not on the anode with its deleterious HER and possible implications. Often new catalysts and cathode concepts are proposed and investigated to propel the much needed research on the sluggish oxygen reduction

Received: September 30, 2019
Accepted: November 15, 2019
Published: December 31, 2019

DOI: 10.1021/acsomega.9b03224
ACS Omega 2020, 5, 626−633

reaction (ORR) and oxygen evolution reaction (OER).[34−41] A recent benchmarking study on anode concepts for Zn−O_2 batteries revealed that 65% of the published research articles during the past 20 years used simple Zn foil anodes in lab-scale research (21 out of 32 articles; see also Table S1 in the Supporting Information), although it is not the state-of-the-art anode and facilitates the HER as the side reaction.[42]

Thus, the purpose of our study is to shed light on the gas that is evolved at the anode during battery testing with the commonly used zinc foil. We aim to gain understanding about the governing factors for the electrochemical formation of hydrogen in practically relevant operating conditions. By means of electrochemical analysis, pressure change measurements, and operando differential electrochemical mass spectrometry (DEMS), we elucidate the implications for the underlying working principle of the battery. In the end, our study might help transfer the gained knowledge to apply improved cycling protocols and setups for testing novel materials for the anode and cathode of zinc−oxygen batteries.

RESULTS AND DISCUSSION

Battery Cycling. Figure 1a shows cycling results obtained at 1.0 mA cm^{-2} for a fixed time limit (1 h discharge followed by 1 h charge). This cycling procedure, known as shallow cycling, is commonly applied for testing the performance of Zn−O_2 batteries (as well as other newly developed batteries in lab-scale; compare Table S1) but does not resemble a practical use case. Stable cycling with flat discharge and charge plateaus for 60 cycles over the course of 120 h (the inset in Figure 1a shows the same cycling within 10 h) can be observed. The corresponding capacity withdrawn is 0.79 mA h for each discharge and charge.

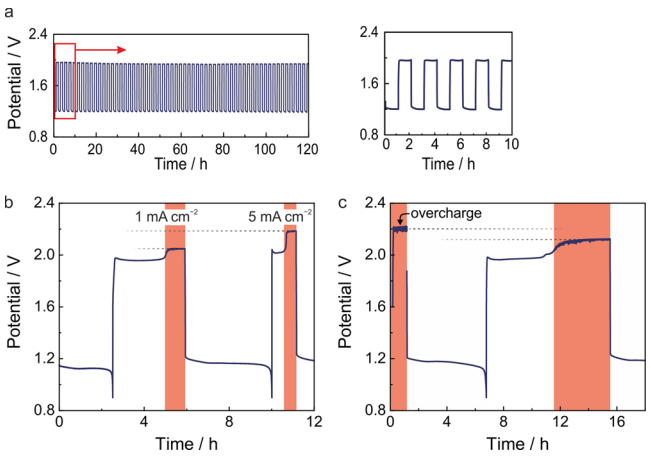

Figure 1. Cycling data of Zn−O_2 batteries with Zn foil as the anode: (a) at 1.0 mA cm^{-2} (discharge/charge step 0.79 mA h, corresponding to a DoD of 0.09%), the inset on the right shows the same cycling within 10 h; (b) first at 1.0 mA cm^{-2} and then at 5.0 mA cm^{-2} (discharge step limited to 0.9 V). The charge step is not limited by a cut-off potential so that—unintentionally—more capacity than previously discharged might be retained during charge. (c) Uncommon cycling protocol starting to charge a pristine, fully charged battery at 1.0 mA cm^{-2}, whereas a second potential plateau above 2.00 V can be observed.

Figure 1b reveals the cycling performance if discharge is not limited by time but rather by potential (cut-off potential at 0.90 V). First, a Zn−O_2 battery is discharged at 1.0 mA cm^{-2} until the cut-off potential is reached at about 2.5 h or 2 mA h. The subsequent charge is yielding the same amount of capacity at a stable potential plateau of about 1.95 V, whereas a second potential plateau emerges from there at 2 mAh (red-colored area).

Next, the cell is discharged again. This time, the charging current is changed to 5.0 mA cm^{-2}. We can observe a first potential plateau exhibiting the same capacity as the preceding discharge with a potential value marginally higher than for 1.0 mA cm^{-2} and a second potential plateau which scales with the current density applied. It is to be noted that we observe only one potential plateau when charging a Zn−O_2 battery with large excess of the electrolyte (compare Figure S2; charging at 10 mA cm^{-2} and 1 mL of electrolyte instead of a few μL). By implication, a large excess of the electrolyte might facilitate other, generally unwanted electrochemical processes, shifting the potential to another plateau, that is, the second plateau.

Figure 1c shows results obtained for a very different cycling protocol that is intentionally chosen to evoke side reactions in the battery: A pristine—and thus fully charged—Zn−O_2 battery is charged further at 1.0 mA cm^{-2}. Thereby, the cell potential increases to values around 2.20 V and is stable for approximately 1 h, corresponding to 0.79 mA h. Afterward, the battery is discharged, achieving approximately 4.38 mA h of discharge capacity. Subsequently, the same amount of capacity is charged at a cell potential of around 1.95 V. After 11.5 h, when the charge capacity is equal to the previously obtained discharge capacity—the cell potential shifts to another plateau above 2.00 V and charge continues steadily, that is, the battery is overcharged. However, the electrons invested during charge must stem from other reactions than the reduction of ZnO so that this mode of operation can not be of interest because it possibly leads to the degradation of the battery itself.

The second potential plateau that appears during the second charging step can also be observed if MnO_2 is used as the catalyst at the cathode instead of the perovskite-type catalyst (compare Figure S3; same cycling profile for a Zn−O_2 cell with commercially available cathode). Furthermore, the second potential plateau does not appear when discharge and charge are limited to a certain threshold value for the cell potential (compare Figure S4; cycling between 0.90 and 2.10 V). It remains to be an open question whether studies employing novel catalyst materials for the cathode of Zn−O_2 batteries do reflect the true impact of the material on the electrochemistry if tested in a two electrode setup.

Gas Analysis. To further understand the underlying processes during charge, we monitored the pressure inside the oxygen reservoir of a closed Zn−O_2 battery and applied operando DEMS analysis for an open cell setup. Figure 2a shows the obtained results for the operando pressure measurement. The constant slope of pressure during discharge is in line with the expected flat plateaus for the cell potential and implies that O_2 is consumed in the oxygen reservoir as intended during ORR. During charge, the pressure increases almost linearly because of the release of O_2 ascribed to the OER. However, at 3.4 mA h of charge (corresponding to ∼9 h of operation; starting point of the charge at the second potential plateau), the slope of the pressure β increases noticeably by a factor of 2.7 from β_1 to β_2, indicating that more gas is formed during charge at the second potential plateau in comparison to the charge at the first plateau.

To enable better comparison and quantification of the slope of the pressure change for a different anode geometry, we divide the slope β by the geometric surface area of the

DOI: 10.1021/acsomega.9b03224
ACS Omega 2020, 5, 626−633

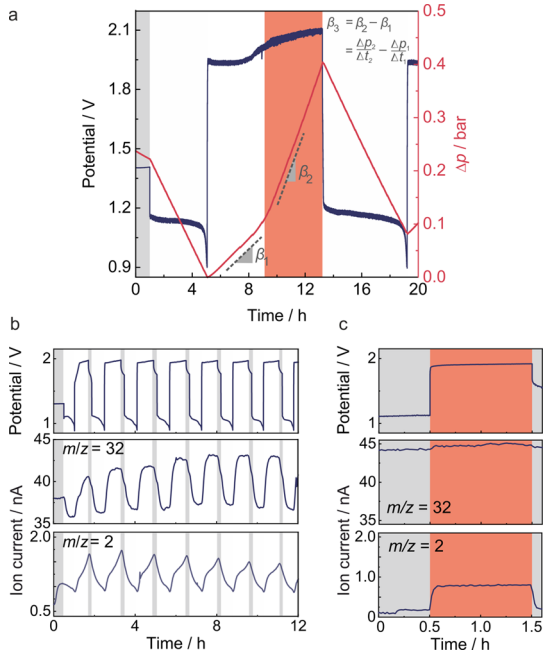

Figure 2. Extended gas analytic during cycling: (a) pressure change in a closed cell system (during cycling at 1.0 mA cm^{-2}). (b) Ion currents for m/z = 32 (assigned to oxygen) and m/z = 2 (assigned to hydrogen) by DEMS (during cycling at 2.5 mA cm^{-2}; raw data in Figures S6, and S7 a). (c) Ion currents for the same m/z values at the OCV mode between 0 and 0.5 h, at 0% DoD, then charging further at 2.5 mA cm^{-2} between 0.5 and 1.5 h, ending in the OCV mode again.

respective anode (Zn foil and Zn sponge as well as Zn particles; see also Figure S5), referred to as β^*.

The value for $\beta_3^* = \beta_2^* - \beta_1^*$ (with β_1^* = 23.56 mbar h^{-1} cm^{-2} and β_2^* = 64.17 mbar h^{-1} cm^{-2}, respectively) obtained during charge at the second potential plateau is approximately 40.61 mbar h^{-1} cm^{-2} and corresponds to approximately 12.94 μmol h^{-1} cm^{-2} of evolved gas—even after ZnO as the designated source of oxygen in the overall cell reaction has been converted completely.

It can be presumed that the additional increase of pressure stems from the formation of hydrogen by means of the well-known electrochemical HER. This assumption is supported by comparing β_3^* to the pressure slope that is obtained for the chemical reaction of H_2O from the electrolyte with the Zn foil anode (only 8.79 mbar h^{-1} cm^{-2} as shown in Figure S5a). The chemical formation of H_2 is much slower compared to the electrochemical formation of H_2 during overcharging the Zn–O_2 battery at 1.0 mA cm^{-2} as shown in Figure 2a. The rate of the electrochemical formation of H_2 increases almost linearly with the current density applied (see Figure S5b; 200.57 mbar h^{-1} cm^{-2} at 5.0 mA cm^{-2}). The finding that the rate of the electrochemical formation of hydrogen is faster than the chemical one is in contrast to the results from Einerhand et al.,[27] whereas they draw their conclusions not from a battery during operation. Besides, a different electrolyte, namely, 8 M KOH saturated with 1 M zincate, is used, for which the amount of zincate in the electrolyte should reduce the activity of H_2O. This relation should diminish the apparent rate of the electrochemical hydrogen evolution.[25]

It is worth mentioning at this point that H_2 evolved in a closed battery system could be used to electrochemically recombine with O_2 at the cathode to form H_2O again: Müller et al. proposed that this intriguing recombination reaction can be used in a large-scale Zn–O_2 battery stack to compensate for large losses of H_2O from the electrolyte because of the HER and Zn corrosion.[52] Deiss et al. included the necessity for overcharging with the benefit of recombination to H_2O into their model-based analysis of Zn–O_2 battery cycling.[53] However, we do not observe that H_2O can be regained in our lab-scale battery setup, indicated by the constant increase in gas pressure during cycling as shown in Figure 2a with the closed battery setup.

The results of the DEMS analysis, shown in Figure 2b, give additional information on the type of gas inside the battery during OCV (open circuit conditions without current flow), discharge, and charge: during OCV, a small amount of H_2 (ascribed to the ion current at m/z = 2) is detected as can be expected from zinc corrosion. The amount of O_2 (ascribed to the ion current at m/z = 32) decreases as expected with an almost constant slope during discharge in each cycle, whereas only a small and constant amount of H_2 is detected. However, a drastic increase of evolved H_2 can be observed in each cycle during charge, while O_2 is evolved and can be detected as expected as well. Even by using a Zn sponge as the state-of-the-art anode, which is doped with In and Bi as inhibitors to suppress HER, we observe the same trend for the evolution of H_2 (compare Figures S7b and S8).

Charging a battery further that is already at 100% state-of-charge after assembly does not show a significant increase of the ion current for O_2 (compare Figure 2c for using a pristine Zn anode). Instead, the ion current ascribed to H_2 is increasing while the battery is charged. This observation implies that the formation of the H_2 species is caused by an electrochemical reaction, which we will further elucidate in the following.

To suppress the formation of H_2, we assembled a Zn–O_2 battery with 800 ppm of polyethylene glycol in the electrolyte (see Figure S10) and recorded the respective pressure change in the O_2 reservoir. Adding a surfactant to the electrolyte decreases the amount of additionally evolved gas in general, which also holds good for our results. Using Zn particles that are surface-treated with indium (In) and bismuth (Bi) or using poly acrylic acid (PAA) as the electrolyte additive does not have a significant impact on the rate of gas evolution during the OCV mode (see Figure S10c). Because further optimization of the electrolyte is out of the scope of this study, we refer the reader to further study about electrolyte additives.[55−59]

Impact of Anode Roughness on Charge. To further shed light on the evolution of H_2 during charge, we apply discharge and charge cycling for a Zn–O_2 battery with a reference electrode. Besides, we use ex situ SEM analysis of the Zn anode to link morphological changes on the electrode surface to the electrochemical results obtained. The results are depicted in Figure 3a,b.

The performed EIS measurements (Figure S11) reveal that the increase of the potential during charge at the second potential plateau is not due to an increase of the internal resistance of the battery. This result and the aforementioned cycling profiles imply that there is a relation between the charge mechanism at the second potential plateau and an increase in overpotential because of the presence of the electrochemically induced HER. For better comparison, the overpotential for the hydrogen evolution on Zn metal is given in a previous study by Lee.[54]

Figure 3a reveals the contribution of each electrode to the full cell potential: the cathode potential remains almost

DOI: 10.1021/acsomega.9b03224
ACS Omega 2020, 5, 626−633

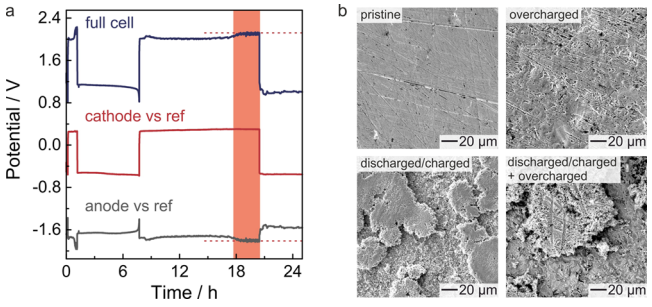

Figure 3. (a) Cycling a Zn−O_2 battery at 1.0 mA cm^{-2} with a Zn foil as the anode and a $Ni(OH)_2$/NiOOH reference electrode soaked with 4 mol dm^{-3} KOH. (b) SEM analysis of the anode in the pristine state and after various steps of cycling (corresponding electrochemical data shown in Figure S9).

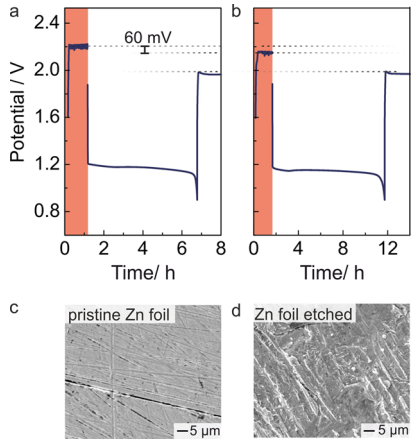

Figure 4. Cycling a Zn−O_2 battery at 1.0 mA cm^{-2} with a Zn foil as the anode starting with charging, whereas the DoD is 0% after assembly: (a) pristine state. (b) Etched Zn foil as the anode (the etching solution was 0.5 M HCl). (c,d) SEM images of the surface of both the pristine and the as-prepared/etched Zn foil anode.

constant during each step of discharge and charge and does not fluctuate. Besides, the overvoltage at the cathode is much higher than for the anode during operation, which is well known for Zn−O_2 batteries.[53] The potential of the anode is not constant during charge at the second potential plateau and fluctuates significantly, which can be correlated to evolving gas bubbles. This random gas formation can decrease the electrochemical active surface area and thus increase the potential at the anode.

The SEM analysis, shown in Figure 3b (corresponding electrochemical data in Figure S9; corresponding elemental analysis of the agglomerates formed is shown in Figure S12), reveals that the surface of the anode has changed during charge at the second potential plateau: a pristine anode possesses a smooth surface with a defined surface area, which leads to cycling with stable cell potentials. After one full discharge/charge cycle, the electrode surface is covered with unevenly distributed agglomerates of Zn and ZnO that have formed randomly during stripping and plating. The structural properties of the agglomerates are investigated by X-ray diffraction analysis (XRD) (results of the analysis for similar cycling data are shown in Figure S13). We observe that indeed ZnO is formed on the anode surface after discharge and that ZnO is formed to a lesser extent for overcharging a battery with a Zn foil anode.

Figure 4 shows that the value of the second potential plateau can be shifted if the surface of the pristine Zn anode is roughened (here intentionally etched with HCl before use; increase in surface roughness between the pristine and the etched state shown in Figure 4b,c). Cycling a battery with the roughened anode surface leads to a decrease in the overpotential during charge at the second potential plateau by 60 mV. The potential at the anode scales with the active surface area: an increased surface area will provide more reaction sites, whereas only the same number of electrons participates in the electrochemical reaction (constant current operation). Thus, more of the reactants in the liquid electrolyte can reach the higher amount of reaction sites, lowering presumably the concentration overpotential and thus yielding a reduced overpotential in total.

H_2 is formed electrochemically from the solvent H_2O during the overcharge of a Zn−O_2 battery, which is in line with previous studies, and is known for decades already.[54,60,61] It is to be noted that the chemical reaction of Zn metal with H_2O is often assumed to be the predominant process.[27,62−64]

In Figure S14, we summarize the reactions known to take place at the anode of the Zn−O_2 battery. It can be presumed that the impact of the electrochemically induced HER[54,60,61] has severe consequences for the cycling of the battery because the reaction consumes solvent water in the aqueous electrolyte. In this view, it might be challenging to estimate the practical cycling stability and lifetime of Zn−O_2 batteries if Zn foil is used as the anode because it enables the consumption of the solvent H_2O in the electrolyte and gas evolution at the same time (compare also Figure S2; charging a cell with a large excess of the liquid electrolyte progresses without a change in the charging plateau). Using defined amounts of the electrolyte instead of an excess electrolyte can help notice whether unwanted overcharge takes place or not—complete consumption of the electrolyte would then yield early battery failure and reasonable, practical cycle numbers.

By implication, testing a novel catalyst material at the cathode by means of a full cell test with the Zn foil anode might not reveal the full impact of the cathode because slight changes on the anode surface (different distributor; variation in surface treating before use) will affect the overall cell potential.

CONCLUSIONS

We aim to extend the already existing knowledge about the evolution of hydrogen during the operation of zinc−oxygen batteries. By applying a comprehensive set of electrochemical measurements, morphology analysis, and gas analytic, we show a link between the evolution of hydrogen and the processes at the anode. We observe by means of DEMS that the ion current signal ascribed to hydrogen is higher during charge than during discharge and conclude that hydrogen mainly stems from a deleterious electrochemical reaction at the anode. This process and its polarization behavior both depend on the current as well as on the surface area of the anode. By implication, some of the electrons used to recharge aqueous zinc−oxygen batteries can be easily dissipated into deleterious side reactions that, in the end, can consume water until the electrolyte is depleted.

The results gained help to put the use of zinc foil as the anode for performance testing of zinc−oxygen batteries into perspective: once all zinc oxide is converted back to zinc, an

DOI: 10.1021/acsomega.9b03224
ACS Omega 2020, 5, 626−633

increase in overpotential due to the presence of the electrochemically induced evolution of hydrogen sets in. The starting point for this increase is not detectable in the electrochemical data if a large excess of the electrolyte is used. The findings can be used to carefully select the testing protocols and cell setups for zinc−oxygen batteries to reveal their true performance and the impact of novel materials introduced.

METHODS

Electrode Preparation. The Zn foil anodes (2 mm thickness, >99.99%, ChemPur, Germany) were polished before use with SiC paper (5 μm, Buehler); the preparation of Zn sponge anodes (used for better comparison to state-of-the-art cycling performance; based on the work by Parker and colleagues[43,44]) and gas diffusion electrodes (GDEs) with the Sr_2CoO_3Cl catalyst was carried out as described previously.[45,46] HCl (0.5 M) (reactant grade) was used to chemically etch off the surface of pristine Zn anodes.

The Zn foil anode is not the state-of-the-art electrode regarding cycling stability and performance but was chosen for the purpose of the herein conducted fundamental study to shed light on the otherwise less-distinct HER during the operation. The reasons for using Zn foil as the anode in Zn−O_2 battery research are as follows: easy handling and cutting to almost any size; no need for additional host material or current collector while providing mechanical stability. On the downside, no full discharge to 100% of the discharge capacity is possible, as well as fast passivation[47,48] with ZnO can occur (compare diminished passivation with 3D-structured and Zn particle anodes).[43,44,49]

Assembly of Zn−O_2 Cells. Zn−O_2 cells were prepared as CR2032 coin-type cells (TOB New Energy Limited) or as in-house-modified Swagelok-type cells (i.e., known as "Giessen cell")[50] using the following assembly protocol: The freshly polished Zn foil (12 mm diameter) anode was placed on top of a tin (Sn) disk current collector (125 μm thickness, 99.99+%, ChemPur, 16 mm diameter for CR2032, 13 mm diameter for Swagelok-type) and covered with 150 μL of 4 mol dm^{-3} KOH aqueous electrolyte. Four laminated (16 mm diameter for CR2032, 13 mm diameter for Swagelok-type) nonwoven separators (Celgard 5550) were soaked in 4 mol dm^{-3} KOH solution and used as the separator between the Zn anode, and the GDE. 800 ppm polyethylene glycol (PEG 600, Sigma-Aldrich) was used as the additive in 4 mol dm^{-3} KOH solution to suppress HER where mentioned. Additional 25 μL of KOH solution (4 mol dm^{-3}) were used to wet the exposed separator membrane surface again before placing the GDE (10 mm diameter) and closing the cell. A titanium mesh (10 mm diameter, 0.076 mm wire thickness, Alfa Aesar) was used as the current collector at the cathode side. As particular modification in the coin-type cell, a stainless steel spacer (15.5 mm diameter, 0.2 mm thick, MTI Corporation) was placed underneath the Sn current collector. The void space between the spacer, Sn current collector, and Zn anode was kept dry, and the infiltration of the electrolyte was prevented by using an insulating tape made of polytetrafluoroethylene. A stainless steel spring (15.4 mm diameter, 1.1 mm thick, MTI Corporation) was on top of the titanium mesh current collector. Finally, the coin cell was automatically closed with a crimping machine at a pressure equivalent to 1 ton per coin cell area (MTI Corporation). A $Ni(OH)_2$/NiOOH reference electrode (Panasonic) was used as the quasi-reference electrode in the three-electrode measurements with a Swagelok-type cell.

To evaluate and report data on Zn−O_2 batteries, guidelines introduced in a very recent perspective article by Parker et al.,[51] were followed.

Pressure Measurement. Time-dependent pressure change inside the gas volume of the Swagelok-type cells was recorded using an PAA-33X absolute pressure sensor, a K104B USB computer adapter (both Omega Engineering), and the software ControlCenterSeries30 (Keller AG) during cycling (compare Figure S1a for the measurement setup).

Electrochemical Characterization. Electrochemical characterization was performed using a SP-300 potentiostat/galvanostat (Biologic) and a BCS-805 battery cycler (Biologic) at room temperature. The Zn−O_2 coin cells were cycled inside a sealed gas container [total volume of approximately 0.5 L, filled with humidified O_2 (purity 5.0, Praxair)]. The Swagelok-type cells—with a gas reservoir of approximately 8 mL—were likewise filled with pure humidified O_2 at 1 bar. Zn−O_2 cells were galvanostatically cycled at ±1.0, 5.0, and 10.0 mA cm^{-2} with the cut-off potential during discharge set to 0.90 V.

Where needed, capacity values referred to in this work are based on the mass of active material Zn used. Overcharging occurs if the mA h/g_{Zn} gained during discharge is gained back in the subsequent charge step, added a surplus amount of mA h/g_{Zn} in capacity.

Differential Electrochemical Mass Spectrometry. Lysgaard et al. used additives on the Zn anode surface and determined the amount of H_2 that was formed by using DEMS by accumulating gas within 1 h of charge for each data point.[21] We apply a continuous flow DEMS setup, that is, an open system to investigate the gas composition in electrically rechargeable Zn−O_2 cells with resolution in time in the range of several minutes (see also Figure S1b for details on the measurement setup). After preparation of the electrodes (Zn foil or Zn sponge, GDE and Sn disk current collector; all 10 mm diameter) and separators (three anion-exchange membranes 16 mm diameter, A-201 (Tokuyama) or nonwoven separators (Celgard 5550) soaked with the electrolyte as previously reported[46]), the cell elements were transferred to a glovebox with a nitrogen atmosphere and assembled as the Zn−O_2 cell as described above. Then, the Zn−O_2 cell was connected to the DEMS setup, which consists of a BaSyTec cycling station for electrochemical analysis, a mass flow controller (control unit PR4000, MKS), and the mass spectroscopy unit (Prisma QMA 200, Pfeiffer Vacuum GmbH). The cell was initially fed with 3.5 mL min^{-1} of synthetic air (80% N_2, 20% O_2) to ensure optimal reactant distribution; the flow was reduced to 0.5 mL min^{-1} after 15 min, allowing an optimal determination of the gas composition. To prevent drying out of the cell, the gas flow was directed through a humidifier (tank with deionized H_2O) and then directed into the cell. For better data visualization, the current signal for m/z = 32 (assigned to oxygen) was drift-corrected because a linear increase of the total ion current I_0—originating from the measurement setup and not from the electrochemical cell—was observed (compare raw data in the Supporting Information).

Scanning Electron Microscopy. Microstructure images of Zn foil anodes (before and after cycling) were obtained on a Merlin high-resolution scanning electron microscope (SEM; Carl Zeiss AG, Germany).

DOI: 10.1021/acsomega.9b03224
ACS Omega 2020, 5, 626−633

Energy-Dispersive X-Ray Spectroscopy. Extended surface analysis by means of energy dispersive X-ray spectroscopy (EDS) mapping was performed with a 50 mm^2 Silicon Drift Detector X-Max (Oxford Instruments) during SEM analysis at the very same samples.

X-Ray Diffraction. An Empyrean X-ray powder diffractometer (Cu Kα, 40 kV, 40 mA; PANalytical) was used to provide structural data on the surface of Zn foil anodes.

■ ASSOCIATED CONTENT

Supporting Information

The Supporting Information is available free of charge at https://pubs.acs.org/doi/10.1021/acsomega.9b03224.

Working principle and expected reactions in alkaline Zn−O_2 batteries; literature survey on the use of Zn foil anodes; experimental cell setup for pressure measurement; experimental cell setup for operando DEMS measurement; discharge and charge cycling of a Zn−O_2 battery, using approximately 1 mL of electrolyte; charge and discharge cycling of a Zn−O_2 battery presenting the second potential plateau using a GDE with the MnO_2 catalyst; charge and discharge cycling of a Zn−O_2 battery using a cycling protocol limited to a discharge potential of 0.90 V and to a charge potential of 2.10 V; recorded pressure change in the closed Swagelok cells in the argon atmosphere during the OCV mode and in the oxygen atmosphere during cycling at 5.0 mA cm^{-2}; recorded ion currents for m/z = 32, m/z = 2, and m/z = 44 by DEMS during cycling and zero current conditions; cycling profiles for SEM-analyzed Zn anodes; charge and discharge cycling of a Zn−O_2 battery and SEM images starting with overcharge of pristine Zn foil and Zn foil etched with 0.5 M HCl; drift correction of originate ion currents; recorded ion currents for m/z = 2 by DEMS during OCV for a Zn−O_2 battery; discharge and charge cycling of a Zn−O_2 battery with PEG 600 as the electrolyte additive and recorded pressure change; pressure change recorded in Swagelok cells containing the zinc anode, separator, and GDE as the cathode with PEG 600, PAA as the electrolyte additive, and In and Bi on top of the Zn particles at zero current conditions applied; results of EIS analysis; extended surface analysis by means of EDS and XRD; schematic on the evolution of hydrogen at the anode surface (PDF)

■ AUTHOR INFORMATION

Corresponding Author

*E-mail: daniel.schroeder@phys.chemie.uni-giessen.de.

ORCID

Kohei Miyazaki: 0000-0001-5177-3570

Daniel Schröder: 0000-0002-2198-0218

Notes

The authors declare no competing financial interest.

■ ACKNOWLEDGMENTS

The authors gratefully acknowledge financial support by the BMBF (Federal Ministry of Education and Research) within the Japanese/German projects “Zisabi” (03XP0086) and “DEMS-BAT” (03XP0085) and by the DFG via the GRK (Research Training Group) 2204 “Substitute Materials for sustainable Energy Technologies”.

■ REFERENCES

(1) Pan, J.; Xu, Y. Y.; Yang, H.; Dong, Z.; Liu, H.; Xia, B. Y. Advanced Architectures and Relatives of Air Electrodes in Zn-Air Batteries. *Adv. Sci.* **2018**, *5*, 1700691.

(2) Gu, P.; Zheng, M.; Zhao, Q.; Xiao, X.; Xue, H.; Pang, H. Rechargeable Zinc−Air Batteries: A Promising Way to Green Energy. *J. Mater. Chem. A* **2017**, *5*, 7651−7666.

(3) Xu, S.; Yao, Y.; Guo, Y.; Zeng, X.; Lacey, S. D.; Song, H.; Chen, C.; Li, Y.; Dai, J.; Wang, Y.; et al. Textile Inspired Lithium-Oxygen Battery Cathode with Decoupled Oxygen and Electrolyte Pathways. *Adv. Mater.* **2018**, *30*, 1704907.

(4) Zhang, S. S. Problem, Status, and Possible Solutions for Lithium Metal Anode of Rechargeable Batteries. *ACS Appl. Energy Mater.* **2018**, *1*, 910−920.

(5) Stock, D.; Dongmo, S.; Damtew, D.; Stumpp, M.; Konovalova, A.; Henkensmeier, D.; Schlettwein, D.; Schröder, D. Design Strategy for Zinc Anodes with Enhanced Utilization and Retention: Electrodeposited Zinc Oxide on Carbon Mesh Protected by Ionomeric Layers. *ACS Appl. Energy Mater.* **2018**, *1*, 5579−5588.

(6) McCloskey, B. D.; Garcia, J. M.; Luntz, A. C. Chemical and Electrochemical Differences in Nonaqueous Li-O2 and Na-O2 Batteries. *Phys. Chem. Lett.* **2014**, *5*, 1230−1235.

(7) Padbury, R.; Zhang, X. Lithium−Oxygen Batteries—Limiting Factors That Affect Performance. *J. Power Sources* **2011**, *196*, 4436−4444.

(8) Li, Y.; Lu, J. Metal-Air Batteries: Will They Be the Future Electrochemical Energy Storage Device of Choice? *ACS Energy Lett.* **2017**, *2*, 1370−1377.

(9) Mahne, N.; Fontaine, O.; Thotiyl, M. O.; Wilkening, M.; Freunberger, S. A. Mechanism and Performance of Lithium−Oxygen Batteries − a Perspective. *Chem. Sci.* **2017**, *8*, 6716−6729.

(10) Song, K.; Agyeman, D. A.; Park, M.; Yang, J.; Kang, Y.-M. High-Energy-Density Metal-Oxygen Batteries: Lithium-Oxygen Batteries vs Sodium-Oxygen Batteries. *Adv. Mater.* **2017**, *29*, 1606572.

(11) McCloskey, B. D.; Burke, C. M.; Nichols, J. E.; Renfrew, S. E. Mechanistic Insights for the Development of Li−O2 Battery Materials: Addressing Li2O2 Conductivity Limitations and Electrolyte and Cathode Instabilities. *Chem. Commun.* **2015**, *51*, 12701−12715.

(12) Conder, J.; Marino, C.; Novák, P.; Villevieille, C. Do Imaging Techniques Add Real Value to the Development of Better Post-Li-Ion Batteries? *J. Mater. Chem. A* **2018**, *6*, 3304−3327.

(13) Pietsch, P.; Hess, M.; Ludwig, W.; Eller, J.; Wood, V. Combining Operando Synchrotron X-Ray Tomographic Microscopy and Scanning X-Ray Diffraction to Study Lithium Ion Batteries. *Sci. Rep.* **2016**, *6*, 27994.

(14) Pinedo, R.; Weber, D. A.; Bergner, B.; Schröder, D.; Adelhelm, P.; Janek, J. Insights into the Chemical Nature and Formation Mechanisms of Discharge Products in Na−O2 Batteries by Means of Operando X-Ray Diffraction. *J. Phys. Chem. C* **2016**, *120*, 8472−8481.

(15) Berkes, B. B.; Jozwiuk, A.; Sommer, H.; Brezesinski, T.; Janek, J. Simultaneous Acquisition of Differential Electrochemical Mass Spectrometry and Infrared Spectroscopy Data for in Situ Characterization of Gas Evolution Reactions in Lithium-Ion Batteries. *Electrochem. Commun.* **2015**, *60*, 64−69.

(16) Ganapathy, S.; Adams, B. D.; Stenou, G.; Anastasaki, M. S.; Goubitz, K.; Miao, X.-F.; Nazar, L. F.; Wagemaker, M. Nature of Li2O2 Oxidation in a Li−O2 Battery Revealed by Operando X-Ray Diffraction. *J. Am. Chem. Soc.* **2014**, *136*, 16335−16344.

(17) Schröder, D.; Bender, C. L.; Arlt, T.; Osenberg, M.; Hilger, A.; Risse, S.; Ballauff, M.; Manke, I.; Janek, J. Operando X-Ray Tomography for next-Generation Batteries: A Systematic Approach to Monitor Reaction Product Distribution and Transport Processes. *J. Phys. D: Appl. Phys.* **2016**, *49*, 404001.

(18) Haas, O.; Müller, S.; Wiesener, K. Wiederaufladbare Zink/Luftsauerstoff-Batterien. *Chem. Ing. Tech.* **1996**, *68*, 524−542.

(19) Caramia, V.; Bozzini, B. Materials Science Aspects of Zinc − Air Batteries : A Review. *Mater. Renew. Sustain. Energy* **2014**, *3*, 1−12.

DOI: 10.1021/acsomega.9b03224
ACS Omega 2020, 5, 626−633

(20) Li, Y.; Dai, H. Recent Advances in Zinc-Air Batteries. *Chem Soc Rev* **2014**, *43*, 5257−5275.
(21) Lysgaard, S.; Christensen, M. K.; Hansen, H. A.; García Lastra, J. M.; Norby, P.; Vegge, T. Combined DFT and Differential Electrochemical Mass Spectrometry Investigation of the Effect of Dopants in Secondary Zinc−Air Batteries. *ChemSusChem* **2018**, *11*, 1933−1941.
(22) Mainar, A. R.; Leonet, O.; Bengoechea, M.; Boyano, I.; de Meatza, I.; Kvasha, A.; Guerfi, A.; Alberto Blázquez, J. Alkaline Aqueous Electrolytes for Secondary Zinc-Air Batteries: An Overview. *Int. J. Energy Res.* **2016**, *40*, 1032−1049.
(23) Cano, Z. P.; Park, M. G.; Lee, D. U.; Fu, J.; Liu, H.; Fowler, M.; Chen, Z. New Interpretation of the Performance of Nickel-Based Air Electrodes for Rechargeable Zinc−Air Batteries. *J. Phys. Chem. C* **2018**, *122*, 20153−20166.
(24) Chakkaravarthy, C.; Waheed, A. K. A.; Udupa, H. V. K. Zinc—Air Alkaline Batteries — A Review. *J. Power Sources* **1981**, *6*, 203−228.
(25) Ravindran, V.; Muralidharan, V. S. Cathodic Processes on Zinc in Alkaline Zincate Solutions. *J. Power Sources* **1995**, *55*, 237−241.
(26) Mirkova, L.; Tsvetkova, C.; Krastev, I.; Monev, M.; Rashkov, S. A Rotating Ring-Disc Electrode Study of the Hydrogen Evolution during Zinc Deposition from Zincate Electrolytes. *Trans. IMF* **1995**, *73*, 44−47.
(27) Einerhand, R. E. F.; Visscher, W. H. M.; Barendrecht, E. Hydrogen Production during Zinc Deposition from Alkaline Zincate Solutions. *J. Appl. Electrochem.* **1988**, *18*, 799−806.
(28) Lee, S.-M.; Kim, Y.-J.; Eom, S.-W.; Choi, N.-S.; Kim, K.-W.; Cho, S.-B. Improvement in Self-Discharge of Zn Anode by Applying Surface Modification for Zn-Air Batteries with High Energy Density. *J. Power Sources* **2013**, *227*, 177−184.
(29) Yano, M.; Fujitani, S.; Nishio, K.; Akai, Y.; Kurimura, M. Effect of Additives in Zinc Alloy Powder on Suppressing Hydrogen Evolution. *J. Power Sources* **1998**, *74*, 129−134.
(30) Drillet, J. F.; Adam, M.; Barg, S.; Herter, A.; Koch, D.; Schmidt, V.; Wilhelm, M. Development of a Novel Zinc/Air Fuel Cell with a Zn Foam Anode, a PVA/KOH Membrane and a MnO/SiOC-Based Air Cathode. *ECS Trans.* **2010**, *28*, 13−24.
(31) Nartey, V. K.; Binder, L.; Kordesch, K. Identification of Organic Corrosion Inhibitors Suitable for Use in Rechargeable Alkaline Zinc Batteries. *J. Power Sources* **1994**, *52*, 217−222.
(32) Müller, S.; Holzer, F.; Haas, O. Development of a 12 V/20 Ah Electrically Rechargeable Zinc-Air Battery. *Selected Battery Topics: Proceedings of the Symposia on Aqueous Batteries*, 1999; Vol. *98−15*; pp 101−110.
(33) Chen, X.; Zhou, Z.; Karahan, H. E.; Shao, Q.; Wei, L.; Chen, Y. Recent Advances in Materials and Design of Electrochemically Rechargeable Zinc-Air Batteries. *Small* **2018**, *14*, 1801929.
(34) Liu, X.; Park, M.; Kim, M. G.; Gupta, S.; Wu, G.; Cho, J. Integrating NiCo Alloys with Their Oxides as Efficient Bifunctional Cathode Catalysts for Rechargeable Zinc-Air Batteries. *Angew. Chem., Int. Ed.* **2015**, *54*, 9654−9658.
(35) Goh, F. W. T.; Liu, Z.; Ge, X.; Zong, Y.; Du, G.; Hor, T. S. A. Ag Nanoparticle-Modified MnO2 Nanorods Catalyst for Use as an Air Electrode in Zinc−Air Battery. *Electrochim. Acta* **2013**, *114*, 598−604.
(36) Bin, D.; Guo, Z.; Tamirat, A. G.; Ma, Y.; Wang, Y.; Xia, Y. Crab-Shell Induced Synthesis of Ordered Macroporous Carbon Nanofiber Arrays Coupled with MnCo2O4nanoparticles as Bifunctional Oxygen Catalysts for Rechargeable Zn-Air Batteries. *Nanoscale* **2017**, *9*, 11148−11157.
(37) Fan, Y.; Ida, S.; Staykov, A.; Akbay, T.; Hagiwara, H.; Matsuda, J.; Kaneko, K.; Ishihara, T. Ni-Fe Nitride Nanoplates on Nitrogen-Doped Graphene as a Synergistic Catalyst for Reversible Oxygen Evolution Reaction and Rechargeable Zn-Air Battery. *Small* **2017**, *13*, 1700099.
(38) Fu, J.; Hassan, F. M.; Zhong, C.; Lu, J.; Liu, H.; Yu, A.; Chen, Z. Defect Engineering of Chalcogen-Tailored Oxygen Electrocatalysts for Rechargeable Quasi-Solid-State Zinc-Air Batteries. *Adv. Mater.* **2017**, *29*, 1702526.
(39) Yu, Q.; Wu, C.; Xu, J.; Zhao, Y.; Zhang, J.; Guan, L. Nest-like Assembly of the Doped Single-Walled Carbon Nanotubes with Unique Mesopores as Ultrastable Catalysts for High Power Density Zn-Air Battery. *Carbon* **2018**, *128*, 46−53.
(40) Li, T.; Lu, Y.; Zhao, S.; Gao, Z.-D.; Song, Y.-Y. Co3O4-Doped Co/CoFe Nanoparticles Encapsulated in Carbon Shells as Bifunctional Electrocatalysts for Rechargeable Zn-Air Batteries. *J. Mater. Chem. A* **2018**, *6*, 3730−3737.
(41) Li, L.; Yang, J.; Yang, H.; Zhang, L.; Shao, J.; Huang, W.; Liu, B.; Dong, X. Anchoring Mn 3 O 4 Nanoparticles on Oxygen Functionalized Carbon Nanotubes as Bifunctional Catalyst for Rechargeable Zinc-Air Battery. *ACS Appl. Energy Mater.* **2018**, *1*, 963−969.
(42) Stock, D.; Dongmo, S.; Janek, J.; Schröder, D. Benchmarking Anode Concepts: The Future of Electrically Rechargeable Zinc−Air Batteries. *ACS Energy Lett.* **2019**, *4*, 1287−1300.
(43) Parker, J. F.; Chervin, C. N.; Pala, I. R.; Machler, M.; Burz, M. F.; Long, J. W.; Rolison, D. R. Rechargeable Nickel−3D Zinc Batteries: An Energy-Dense, Safer Alternative to Lithium-Ion. *Science* **2017**, *356*, 415−418.
(44) Parker, J. F.; Nelson, E. S.; Wattendorf, M. D.; Chervin, C. N.; Long, J. W.; Rolison, D. R. Retaining the 3D Framework of Zinc Sponge Anodes upon Deep Discharge in Zn-Air Cells. *ACS Appl. Mater. Interfaces* **2014**, *6*, 19471−19476.
(45) Miyahara, Y.; Miyazaki, K.; Fukutsuka, T.; Abe, T. Strontium Cobalt Oxychlorides: Enhanced Electrocatalysts for Oxygen Reduction and Evolution Reactions. *Chem. Commun.* **2017**, *53*, 2713−2716.
(46) Stock, D.; Dongmo, S.; Miyazaki, K.; Abe, T.; Janek, J.; Schröder, D. Towards Zinc-Oxygen Batteries with Enhanced Cycling Stability: The Benefit of Anion-Exchange Ionomer for Zinc Sponge Anodes. *J. Power Sources* **2018**, *395*, 195−204.
(47) Bockelmann, M.; Becker, M.; Reining, L.; Kunz, U.; Turek, T. Passivation of Zinc Anodes in Alkaline Electrolyte: Part I. Determination of the Starting Point of Passive Film Formation. *J. Electrochem. Soc.* **2018**, *165*, A3048−A3055.
(48) Bockelmann, M.; Becker, M.; Reining, L.; Kunz, U.; Turek, T. Passivation of Zinc Anodes in Alkaline Electrolyte: Part II. Influence of Operation Parameters. *J. Electrochem. Soc.* **2019**, *166*, A1132−A1139.
(49) Arlt, T.; Schröder, D.; Krewer, U.; Manke, I. In operando monitoring of the state of charge and species distribution in zinc air batteries using X-ray tomography and model-based simulations. *Phys. Chem. Chem. Phys.* **2014**, *16*, 22273−22280.
(50) Bender, C. L.; Hartmann, P.; Vračar, M.; Adelhelm, P.; Janek, J. On the Thermodynamics, the Role of the Carbon Cathode, and the Cycle Life of the Sodium Superoxide (NaO2) Battery. *Adv. Energy Mater.* **2014**, *4*, 1301863.
(51) Parker, J. F.; Ko, J. S.; Rolison, D. R.; Long, J. W. Translating Materials-Level Performance into Device-Relevant Metrics for Zinc-Based Batteries. *Joule* **2018**, *2*, 2519−2527.
(52) Müller, S.; Holzer, F.; Haas, O.; Schlatter, C.; Comniellis, C. Development of Rechargeable Monopolar and Bipolar Zinc/Air Batteries. *Chim. Int. J. Chem.* **1995**, *49*, 27−32.
(53) Deiss, E.; Holzer, F.; Haas, O. Modeling of an Electrically Rechargeable Alkaline Zn-Air Battery. *Electrochim. Acta* **2002**, *47*, 3995−4010.
(54) Lee, T. S. Hydrogen Over Potential on Pure Metals in Alkaline Solution. *J. Electrochem. Soc.* **1971**, *118*, 1278.
(55) Mirkova, L.; Tsvetkova, C.; Krastev, I.; Monev, M.; Rashkov, S. A Rotating Ring-Disc Electrode Study of the Hydrogen Evolution during Zinc Deposition from Zincate Electrolytes. *Trans. IMF* **1995**, *73*, 44−47.
(56) Mainar, A.; Colmenares, L.; Grande, H.-J.; Blázquez, J. Enhancing the Cycle Life of a Zinc−Air Battery by Means of Electrolyte Additives and Zinc Surface Protection. *Batteries* **2018**, *4*, 46.

DOI: 10.1021/acsomega.9b03224
ACS Omega 2020, 5, 626−633

(57) Mitha, A.; Yazdi, A. Z.; Ahmed, M.; Chen, P. Surface Adsorption of Polyethylene Glycol to Suppress Dendrite Formation on Zinc Anodes in Rechargeable Aqueous Batteries. *ChemElectroChem* **2018**, *5*, 2409−2418.
(58) Sun, K. E. K.; Hoang, T. K. A.; Doan, T. N. L.; Yu, Y.; Zhu, X.; Tian, Y.; Chen, P. Suppression of Dendrite Formation and Corrosion on Zinc Anode of Secondary Aqueous Batteries. *ACS Appl. Mater. Interfaces* **2017**, *9*, 9681−9687.
(59) Lee, C. W.; Eom, S. W.; Sathiyanarayanan, K.; Yun, M. S. Preliminary Comparative Studies of Zinc and Zinc Oxide Electrodes on Corrosion Reaction and Reversible Reaction for Zinc/Air Fuel Cells. *Electrochim. Acta* **2006**, *52*, 1588−1591.
(60) Gabe, D. R. The Role of Hydrogen in Metal Electrodeposition Processes. *J. Appl. Electrochem.* **1997**, *27*, 908−915.
(61) Cho, Y.-D.; Fey, G. T.-K. Surface Treatment of Zinc Anodes to Improve Discharge Capacity and Suppress Hydrogen Gas Evolution. *J. Power Sources* **2008**, *184*, 610−616.
(62) Jung, K.-N.; Jung, J.-H.; Im, W. B.; Yoon, S.; Shin, K.-H.; Lee, J.-W. Doped Lanthanum Nickelates with a Layered Perovskite Structure as Bifunctional Cathode Catalysts for Rechargeable Metal-Air Batteries. *ACS Appl. Mater. Interfaces* **2013**, *5*, 9902−9907.
(63) Wang, R.; Yang, Z.; Yang, B.; Fan, X.; Wang, T. A Novel Alcohol-Thermal Synthesis Method of Calcium Zincates Negative Electrode Materials for Ni-Zn Secondary Batteries. *J. Power Sources* **2014**, *246*, 313−321.
(64) Xu, M.; Ivey, D. G.; Xie, Z.; Qu, W. Rechargeable Zn-Air Batteries: Progress in Electrolyte Development and Cell Configuration Advancement. *J. Power Sources* **2015**, *283*, 358−371.

DOI: 10.1021/acsomega.9b03224
ACS Omega 2020, 5, 626−633